INL/CON-11-23261
PREPRINT

Isothermal Air Ingress Validation Experiments

NURETH-14

Chang H. Oh
Eung S. Kim

September 2011

The INL is a
U.S. Department of Energy
National Laboratory
operated by
Battelle Energy Alliance

ISOTHERMAL AIR INGRESS VALIDATION EXPERIMENTS

Chang H. Oh and Eung S. Kim
Idaho National Laboratory
P.O. Box 16125, Idaho Falls, ID.83415
Chang.Oh@inl.gov, Eungsoo.Kim@inl.gov

Abstract

Idaho National Laboratory carried out air ingress experiments as part of validating computational fluid dynamics (CFD) calculations. An isothermal test loop was designed and set to understand the stratified-flow phenomenon, which is important as the initial air flow into the lower plenum of the very high temperature gas cooled reactor (VHTR) when a large break loss-of-coolant accident occurs. The unique flow characteristics were focused on the VHTR air-ingress accident, in particular, the flow visualization of the stratified flow in the inlet pipe to the vessel lower plenum of the General Atomic's Gas Turbine-Modular Helium Reactor (GT-MHR). Brine and sucrose were used as heavy fluids, and water was used to represent a light fluid, which mimics a counter current flow due to the density difference between the stimulant fluids. The density ratios were changed between 0.87 and 0.98. This experiment clearly showed that a stratified flow between simulant fluids was established even for very small density differences. The CFD calculations were compared with experimental data. A grid sensitivity study on CFD models was also performed using the Richardson extrapolation and the grid convergence index method for the numerical accuracy of CFD calculations . As a result, the calculated current speed showed very good agreement with the experimental data, indicating that the current CFD methods are suitable for predicting density gradient stratified flow phenomena in the air-ingress accident.

Keywords: VHTR, air ingress, CFD code validation.

Introduction

A loss-of-coolant accident (LOCA) is considered an important phenomenon for a very high temperature reactor (VHTR) according to the phenomena identification ranking table (PIRT). Following helium depressurization, it is anticipated that, unless countermeasures are taken, air ingress can be a serious problem, depending on the design, the location, and the orientation of the break.

The Idaho National Laboratory under auspices of the U.S. Department of Energy has performed research and development that focuses on key phenomena that may occur in the Next Generation Nuclear Plant (NGNP)/Generation IV VHTR (Oh and Kim, 2011a, and Oh *et al.*, 2011b). PIRT studies have identified the air ingress event, following on the heels of a VHTR depressurization, as very important (Schultz *et al.*, 2006). Consequently, the development of advanced air ingress-related models and verification and validation requirements are high priorities for the NGNP Program.

The VHTR is a graphite-moderated, uranium-fueled, helium-cooled reactor using a direct or an indirect Brayton or Rankin cycle to convert the heat generated by nuclear fission into electrical energy by means of a helium or steam turbine. High temperature gas-cooled reactor (HTGR) technology has been researched and developed since the 1950s. The VHTR produces a higher outlet temperature than the HTGR. VHTRs work on the principle of passing a cooling gas through the core, then running the heated gas directly to a steam generator or a gas turbine. VHTRs have been built in Japan and China for their nuclear research. VHTRs have several advantages over light water reactors, including fuel integrity, proliferation resistance, a relatively simple fuel cycle, easy refueling, and modularity to supply electricity to remote areas. Even though gas reactors have been developed in the past with limited success, the innovations of modularity and integrated state-of-the-art safety systems make the VHTR design attractive from a technical and economic perspective.

The work summarized in this paper is centered on describing the experimental testing of the isothermal air ingress experiments performed at the Idaho National Laboratory.

1. EXPERIMENTAL STUDY ON THE STRATIFIED FLOW

Isothermal Stratified Flow Experiment

The current section describes separate-effect experiments for understanding stratified flow phenomena in the air-ingress accident and for generating data for validation of computer codes, including CFD codes or system analysis codes. This experiment is aimed at the phenomena that occur for a double-ended-guillotine break (DEGB) scenario. Although the DEGB scenario is recognized as a beyond design basis accident (BDBA) scenario, stratified

flow air ingress experiments are being conducted to study this experimental break configuration because: (i) it is a limiting event and reactor safety-related limiting calculations are required to be included by the U.S. Nuclear Regulatory Commission for its licensing application, and (ii) the geometry is considerably simpler than the more likely small leak scenarios of which experimental work and CFD simulation will be performed later. .
Density gradient driven flow is a new issue in the VHTR safety analysis field. The detailed mechanisms for the whole scenario have not yet been fully understood or validated up to the level of satisfaction for the safety analyses. This section summarizes the objective of this experiment.

Experimental Set-up

Air-ingress experiments of a gas-cooled reactor were conducted using a scaled-down test apparatus based on the General Atomics GTMHR design. The DEGB was considered to be the worst case of the air ingress accident. A pipe break accident scenario that mimics the DEGB was demonstrated by opening a pneumatic knife gate valve. The pressure and temperature were measured by transducers on each cylinder for pressure and by thermocouples for temperature measurements. Flow visualization was recorded by a video camera. The operating conditions were ambient pressure and temperature.
The experiments mimicked air ingress into a typical NGNP gas-cooled reactor lower plenum as a countercurrent air and helium flow when the inlet pipe break occurs in the hot duct. A liquid system with water, salt water, or water-sucrose was used. The liquid-liquid system data was used for validating the computational fluid dynamic models.

Figure 1-1 shows the experimental set-up. This experiment consists of two tanks, two horizontal pipes, and a gate valve for separation of two tanks. The horizontal pipe diameter and length were designed to be 0.2 m and 1.0 m, respectively. The tank diameter was 0.9 m, and the height was 1.0 m. Initially, the gate valve was closed, and water and brine filled the two tanks, respectively. The height of the brine and the water at the initial condition were about one-third of the full tank height (= 0.3 m). After achieving a predetermined condition, the experiment was started by opening the gate valve with an 80 psi compressed air. The valve was pneumatically controlled by a solenoid valve. The gate opening size is the same size of the horizontal pipe to avoid flow distortion when liquid flows through the gate valve.

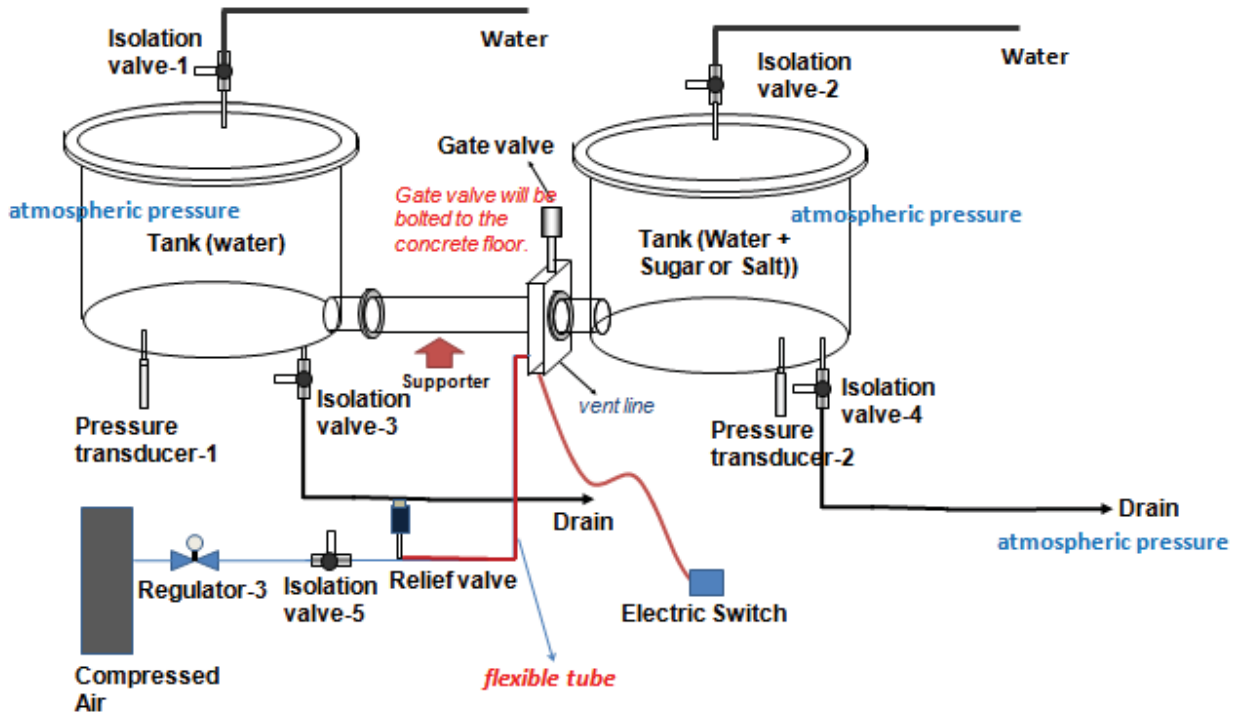

Figure 1-1. Schematics of isothermal DEGB experiment.

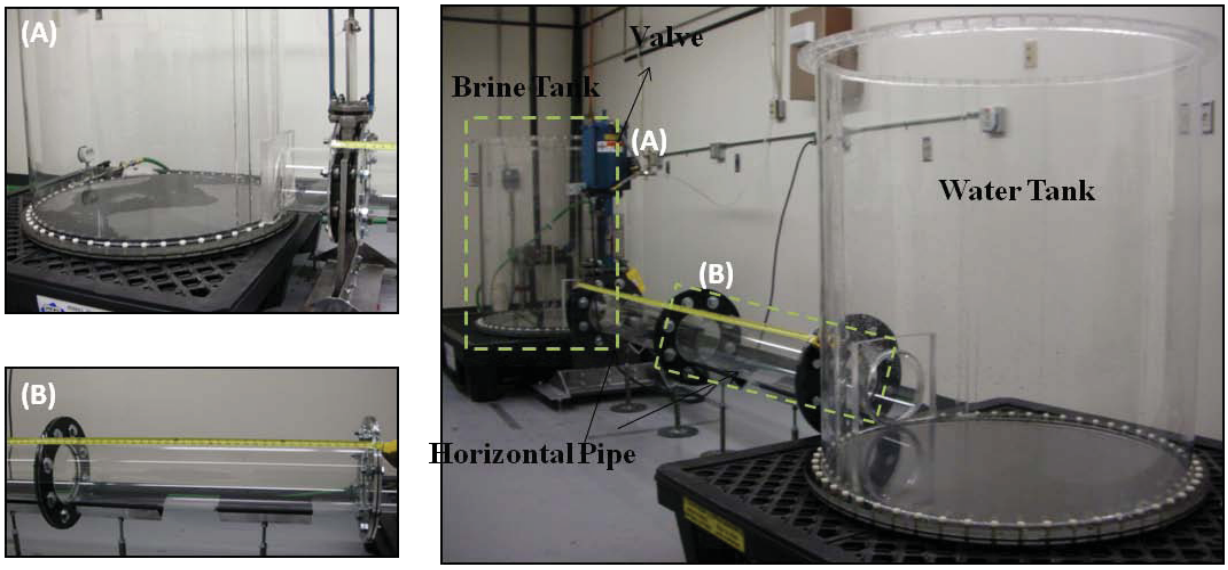

Figure 1-2. Isothermal stratified flow experimental set-up for brine-water.

Figure 1-3 shows the gate valve installed in the test section. This gate valve is actuated by compressed air. The compressed air is controlled by a solenoid valve and an electrical switch. The valve is vertically oriented and mounted on the concrete floor. Figure 1-4 shows the overall set-up of the test facility.

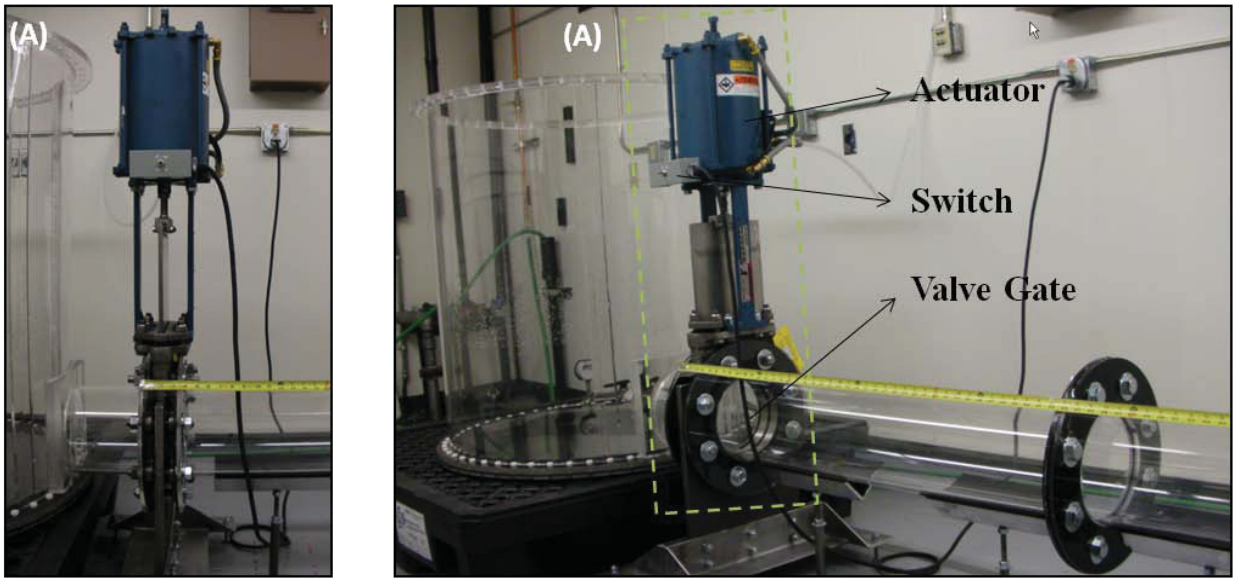

Figure 1-3. Gate valve installation.

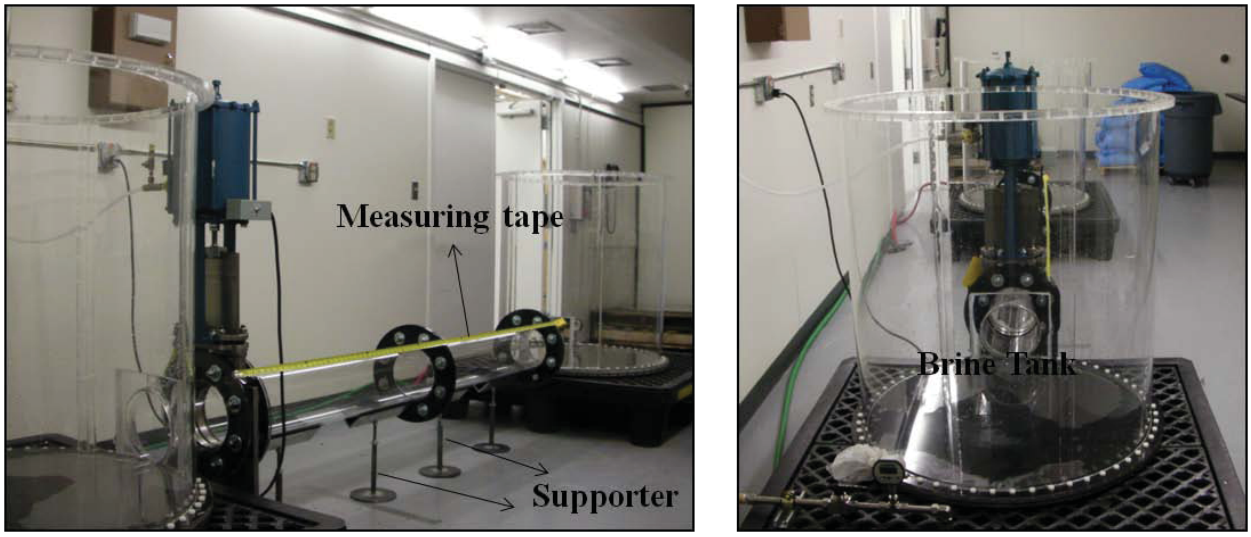

Figure 1-4. Overall set-up of isothermal experiment.

Table 1-1 shows the test matrix of this experiment. The experiment used brine and sucrose as heavy fluids, and water and air as light fluids. The density ratios are changed between 0.98 and 0.866, except for the air/water experiment. The total number of test cases is 9, including the air and water experiment. This experiment covers Reynolds numbers from 2.3×10^4 to 3.79×10^5. Therefore, the main flow is in the turbulent flow regime, which is the same as predicted in the real air-ingress accident. In this regime, the gravity current or density gradient stratified flow is not affected by viscous effect.

Before starting the experiment, the fluid's densities (specific gravity) were measured by a hydrometer. Later, the brine and sucrose were separately sampled for validating measurement. Figure 1-5 shows the brine and sucrose samples taken in a small bottle. In each sample, fluid types and measuring date were written on the bottle surface.

Table 1-1. Experimental conditions and case summary.

	Heavy Fluid	Light Fluid	Heavy Fluid Density (kg/m^3)	Light Fluid Density (kg/m^3)	Density Ratio
Case 1	Sugar	Water	1020	1000	0.980
Case 2	Sugar	Water	1025	1003	0.979
Case 3	Salt	Water	1045	1002	0.959
Case 4	Sugar	Water	1061	1002	0.944
Case 5	Sugar	Water	1080	1002	0.928
Case 6	Sugar	Water	1100	1000	0.909
Case 7	Salt	Water	1130	1002.5	0.887
Case 8	Sugar	Water	1155	1000	0.866
Case 9	Water	Air	1000	1.2	0.0012

Figure 1-5. Brine and sucrose samples.

Experimental Results and Discussions

Figure 1-6 shows the heavy-fluid current propagation through the horizontal pipe for Case 8 (water-sucrose, density ratio = 0.866). In this case, the heavy-fluid was sucrose, and the light-fluid was water. The density ratio was 0.866, which means that the sucrose is about 13.4% heavier than the water. As shown in Figure 1-6, the current rapidly propagates through the pipe, occupying about one-half of the pipe diameter. This result is consistent with the previous observations reported for the lock exchange flow in the Boussinesq flow regimes. In Case 8, the heavy current travelling speed was estimated to be ~0.26 m/s.

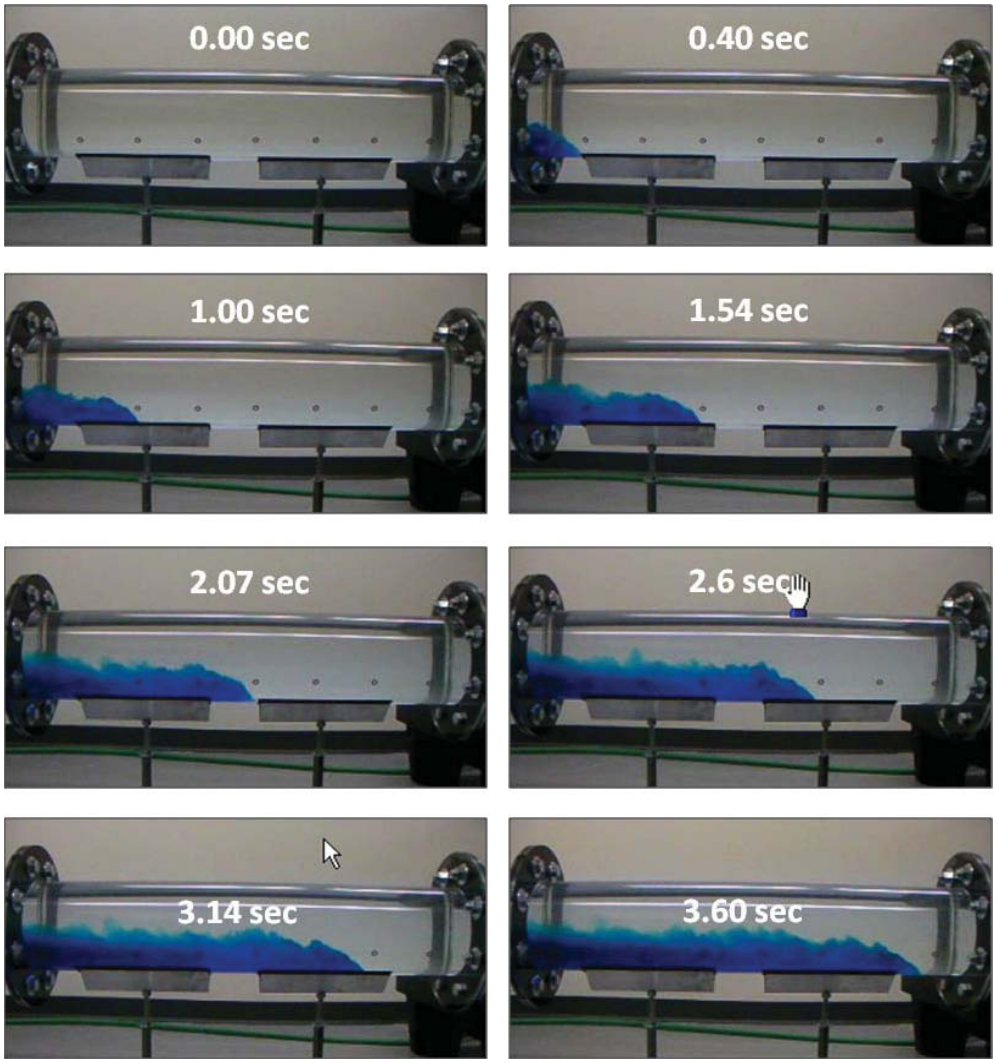

Figure 1-6. Progress of gravity current and stratified flow (water-sucrose, density ratio = 0.866 (Case 8)).

The experimental results are summarized in Table 1-2 and Figure 1-7. The first column in Table 1-2 represents the traveling distance, which was determined by measuring marking spots. The columns from the second to the end show the traveling time when the current arrived at the marking spots. Figure 1-7 plots these data. As shown, the traveling distance has a linear relationship with the traveling time. It means that the heavy current speed is constant throughout the axial direction of the horizontal pipe. This is because of the high Reynolds numbers of the gravity current. For high Reynolds numbers, inertia force dominates viscous effects, so the flow can be considered as an inviscid flow, indicating that the frictional loss can be ignored. The current speed can be calculated by an inverse of the slope of each dataset. As shown in the figure, the current speed is significantly affected by density ratios. The lowest density ratio is 0.866 and the largest is 0.98 for the liquid-liquid experiment. The velocity difference between these two cases are about a factor of 2.5 ($V_{r=0.866}$ = 0.254 m/s, and $V_{r=0.98}$ = 0.101 m/s). If the density ratio is small (the density differences are large), the current speed is fast because of the larger density gradient. The current speed (V = 1.69 m/s) for the air-water experiment was estimated to be even an order faster than for the liquid-liquid experiment.

Table 1-2. Experimental results (traveling distance [x] vs. time).

x (m)	Case 1 time (s)	Case 2 time (s)	Case 3 time (s)	Case 4 time (s)	Case 5 time (s)	Case 6 time (s)	Case 7 time (s)	Case 8 time (s)	Case 9 time (s)
0	0	0	0	0	0	0	0	0	0
0.127	1.54	1.13	0.67	0.73	0.53	0.47	0.5	0.4	—
0.254	3.2	2.3	1.6	1.47	1.26	1	1.2	1	—
0.381	4.54	3.6	2.54	2.2	2.06	1.54	1.8	1.54	—
0.508	5.6	4.9	3.6	2.93	2.66	2.07	2.47	2.07	—
0.635	6.74	5.8	4.87	3.8	3.33	2.6	3.07	2.6	—
0.762	8	7	5.94	4.6	4	3.14	3.6	3.14	—
0.889	9.14	8	6.94	5.4	4.66	3.74	4.14	3.6	—
1.016	10.07	8.87	7.67	6.13	5.13	4.14	4.54	4	0.6

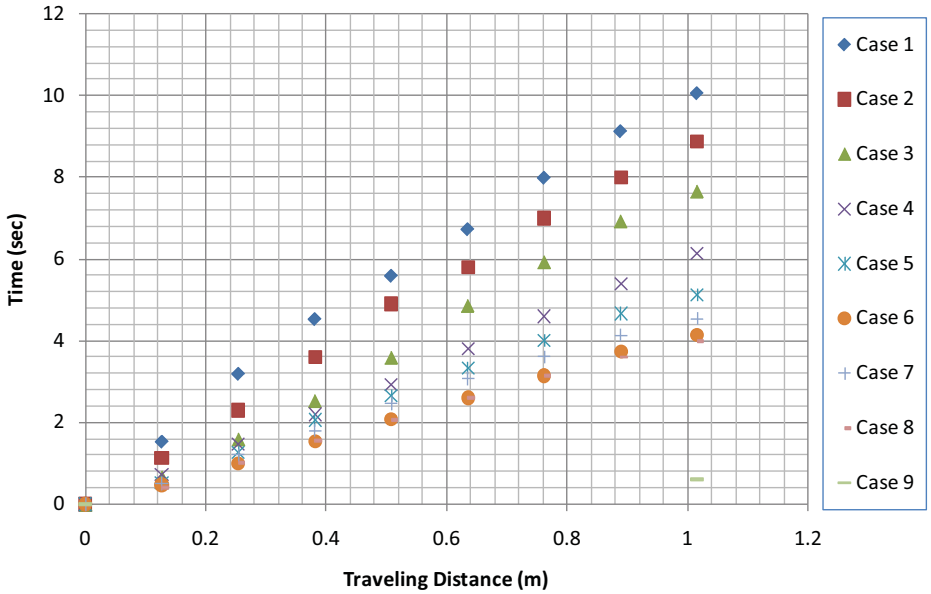

Figure 1-7. Experimental results (traveling distance vs. time).

Table 1-3 summarizes the estimated current speeds between the experiments and theoretical estimations. The heavy current speeds in this experiment range between 0.101 and 1.69 m/s. As shown in the table, the theoretical estimation is in good agreement with the experimental data (within 10% error) for all the cases. The comparisons between the experiment and the theoretical models are discussed in more detail in the next section.

Table 1-3. Comparisons of current speeds between experiment and Benjamin's theoretical model.

Velocity (m/s)	Case 1	Case 2	Case 3	Case 4	Case 5	Case 6	Case 7	Case 8	Case 9
Experiment	0.1009	0.1155	0.1375	0.1657	0.1814	0.2241	0.2381	0.254	1.69
Theory	0.1028	0.1145	0.146	0.1705	0.191	0.2127	0.237	0.26	1.68
Error (%)	1.88	0.86	6.18	2.89	5.29	5.08	0.46	2.36	0.59

2. Validation of CFD Code for Stratified Flow

Computational fluid dynamics methods for a gravity current flow were validated by analyzing CFD and comparing the results with experimental data. Details of this validation are described in this section.

Preliminary CFD Result and Validation Study with Experiment

FLUENT 6.3.26 was used to understand stratified flow in small density ratio cases (from Case 1 to Case 8 in the isothermal experiment). Figure 2-1indicates the overall geometry of the present CFD model of isothermal experiment simulations.

< Overall geometry of CFD model >

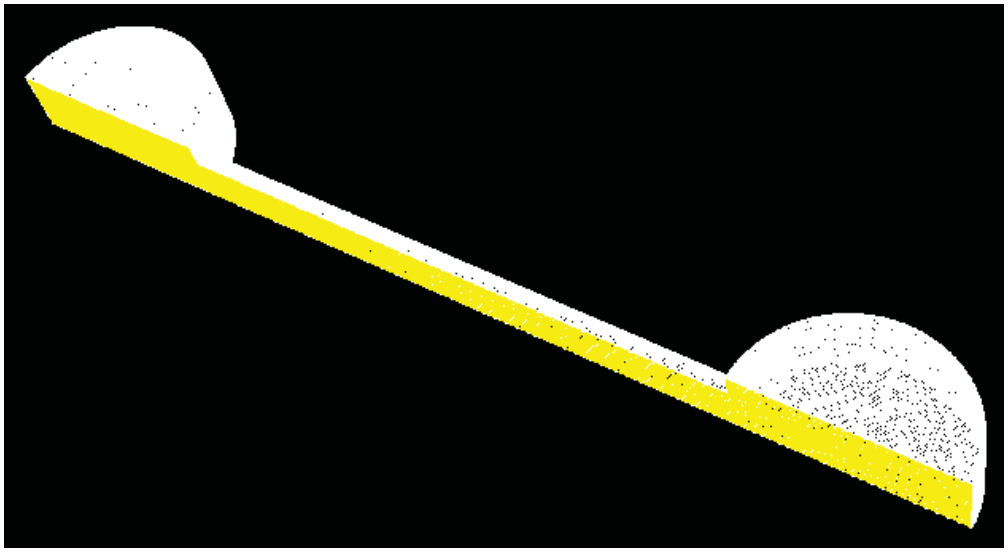

< Side view of model >

Figure 2-1. Overall geometry with normal mesh and side view from symmetry surface.

A 3-D model was developed to simulate the air-ingress phenomena using the INL experimental setup. The overall geometry of the CFD model used for the experiment consisted of three basic parts as shown in Figure 2-1: a heavy fluid brine or sucrose tank (upper left), a light fluid water

or air tank (lower right), and a connecting pipe (going between the two tanks). Three different types of polyhedral meshes (coarse, normal, and fine) were generated and used for the grid sensitivity and convergence study. The first 3-D model developed used a coarse mesh with appropriate grid sizes. Rediscretization with half of coarse mesh grid spacing (normal mesh) and finer meshes were then used as part of Richardson extrapolation method.
The Fluent specification and model used in this simulation are listed as follows:

- Solver:
  - Solver: pressure based
  - Formulation: implicit
  - Space: 3-D double precision
  - Time: unsteady
  - Velocity formulation: absolute
  - Gradient I option: green-gauss cell based
  - Unsteady formulation: 2^{nd} – order implicit
  - Pressurevelocity coupling: PISO
- Discretization:
  - Pressure: PRESTO!
  - Momentum: 2^{nd}-order upwind
  - Turbulent kinetic energy: 2^{nd}-order upwind
  - Turbulent dissipation rate: 2^{nd}-order upwind
  - Species: 2^{nd}-order upwind
  - Energy: 2^{nd}-order upwind
- Viscous Model:
  - Turbulence model: realizable k-e
  - Wall function: standard wall function
- Energy equation
- Species transport model:
  - Mixture material: Mixturetemplate
  - 2 species: water and brine
- Species transport model:
  - Mixture material: Mixturetemplate.

Figure 2-2 shows the initial condition. The left side is filled with brine water that is slightly heavier than pure water density (red: heavy fluid), and right side is filled with pure water (blue: light fluid). Therefore, as transient simulation starts, the heavy fluid intrudes into the light fluid by driving force of density-driven current, which is also defined as stratified flow. Initial conditions for temperature and pressure of both fluids were set as 300 K and 1 atm. identically.

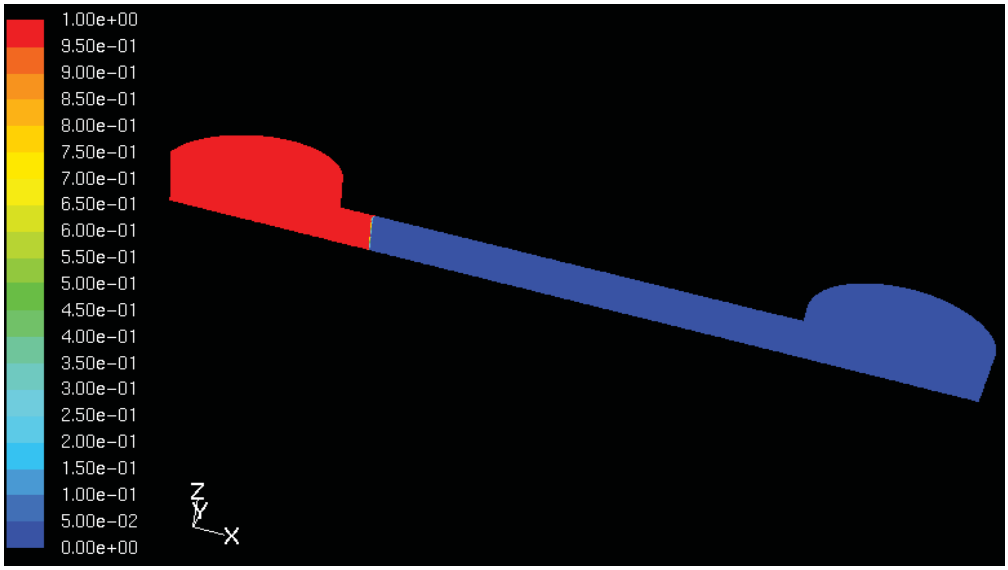

Figure 2-2. Initial brine-water mass fraction (red: brine, blue: water).

3. Grid Refinement Study

As mentioned in the previous section, the grid refinement study was conducted for CFD validations of the spatial dimension and for better prediction of interest variable (front-head speed). The calculation method for front-head speeds in different mesh types (coarse, normal, and fine) is defined with the same method used in the experimental section. Figure 2-3, Figure 2-4, and Figure 2-5 show brine water intrudes into pure water in three mesh-type simulations. As shown in the figures, more blur interface line is observed in coarse meshes, and more sharpness and distinctive interface lines are shown in finer meshes. This sharpness affects front-head position determination, and gives accuracy on front-head speed calculation. An early propagation in Figure 2-5 shows wavy motions, which are captured for initial perturbation in finer meshes. The proper mesh quality provides a more reliable CFD calculation as well as validation. However, the finer mesh requires more computing time. In this section, eight experiment measurement data (from Case 1 to Case 8) are compared with the CFD calculation using the asymptotic approach. It is expected the computing cost will be very high. A solution that avoids this problem is discussed in the next section.

The locations of front heads were determined in this experiment by observing a video clip taken downstream of the current flow, front head, and some billows. So, the front-head positions in simulations were also calculated by the brine water mass fraction at the bottom of pipe channel. Figure 2-6 shows that the mass fraction of brine ranges from 0 to 1. The front head speed was estimated using the distance from one position to others in the travel timing, which is superimposed on the front head (0.5 brine mass fraction in Figure 2-6).

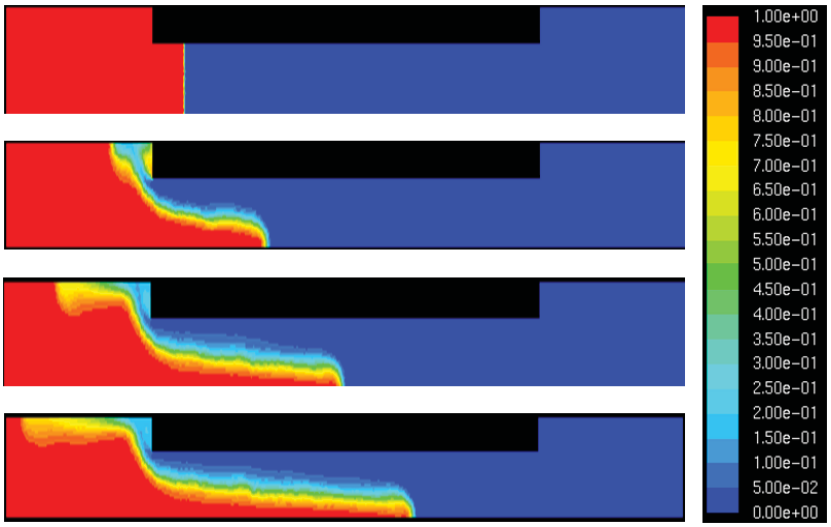

Figure 2-3. Brine intrusion simulation with coarse mesh.

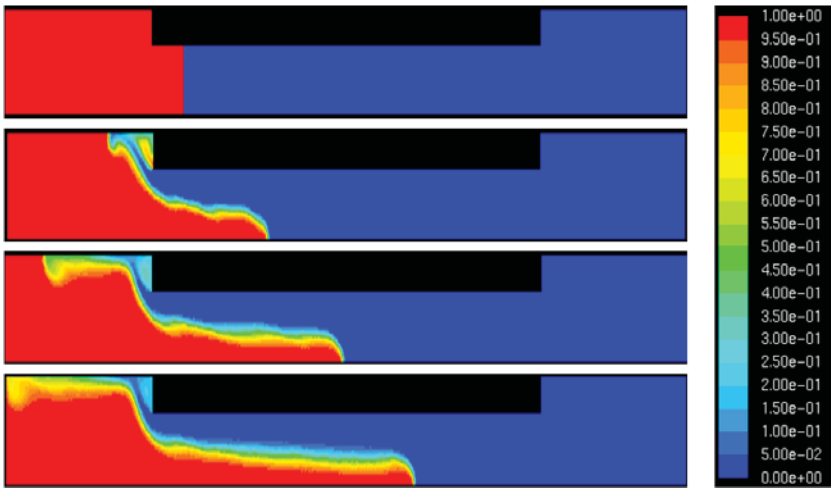

Figure 2-4. Brine intrusion simulation with normal mesh.

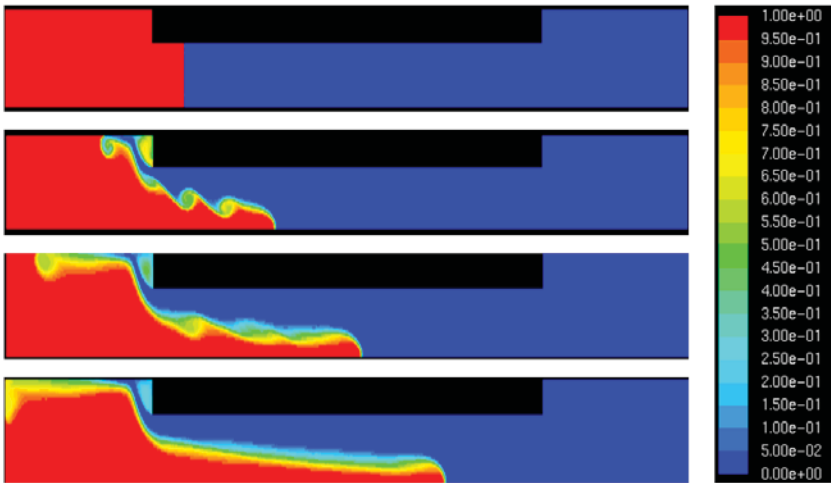

Figure 2-5. Brine intrusion simulation with fine mesh.

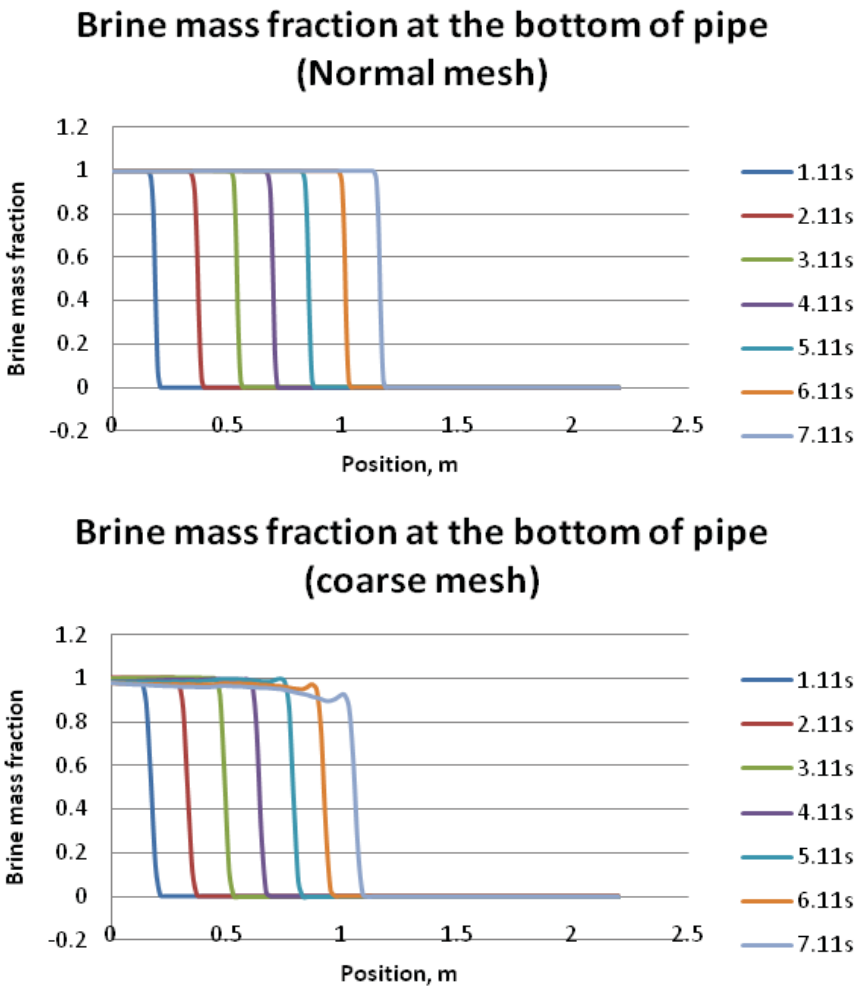

Figure 2-6. Brine mass fraction at the bottom as time marches until 7 sec (normal, coarse mesh)

Normal mesh was found to have better distinctive interface between brine and water compared to coarse mesh. From Figure 2-6, using normal mesh, the edges of the brine or head of the intrusion fluid is well defined, and it is easy to determine half of the brine mass fraction because of this sharp interface. The accumulated numerical diffusion in normal mesh is considered smaller than the accumulated numerical diffusion in coarse mesh, which leads to better sharpening of the interface at normal mesh. It is also observed that more blurriness and less sharpening are found at the edge interface in the small density-difference case because the density-driven driving force is degraded by smaller density differences. Figure 2-7 compares the calculated intrusion-front speeds for three different mesh qualities. As shown, the calculated intrusion-front speed varies by mesh types. In order to have different mesh types, a coarse mesh is first defined with appropriate grid size, rediscretization is performed with half of the coarse mesh gird spacing (normal mesh), and fine mesh is generated out of normal by conducting rediscretization. The ratio of total cell number of normal (fine) mesh to that of coarse (normal) mesh is not exactly eight because the CFD model is a full 3-D unstructured grid. It is, therefore, more appropriate to use normalized grid spacing for a refinement study in the unstructured grid case.

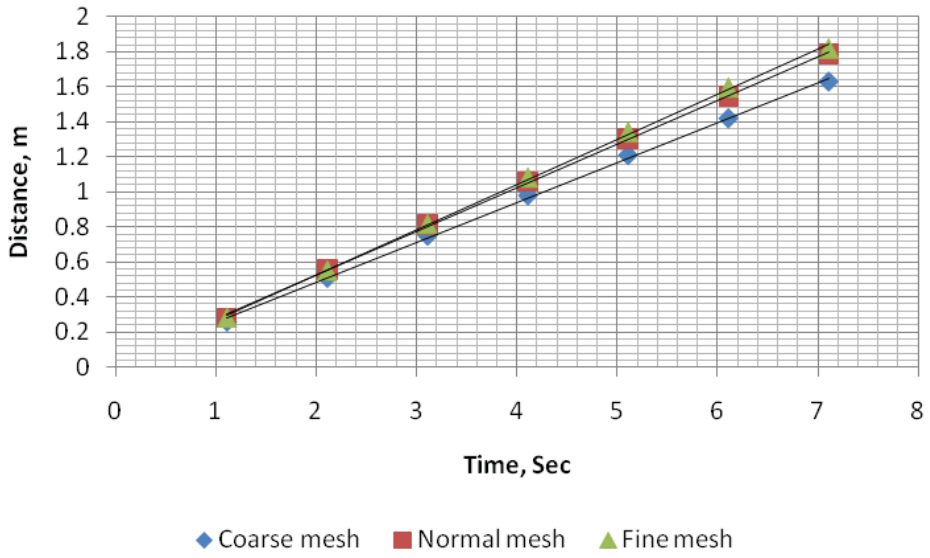

Figure 2-7. Front speed calculation in different mesh (coarse, normal, and fine).

Validating the CFD front-head speed prediction by comparing FLUENT calculation with INL isothermal experimental data (as described in the previous section), INL conducted eight sets of isothermal stratified flow tests for liquid-to-liquid having different fluid densities. Heavy liquid density varies from 1.020 to 1.155 kg/m^3. One significant driving force of stratified flow is density difference – different densities of brine water with pure water generate different current speeds. Figure 1-7 and

Table 1-3 summarize the current speeds of heavy fluids.

The previous subsection showed three sets of FLUENT calculations with coarse, normal, and fine meshes to determine asymptotic front-head speed. Although these three sets of different grid size models provide a good way to calculate asymptotic front-head speed, it requires tremendous computing time to validate each case, especially the fine mesh model, which consumes more than 72 hours of computing time for 20 seconds of transient simulation. Computing time versus accuracy is a key issue in that is well understood in validating CFDs. However, in this experiment, the overall flow behavior was consistent with different fluid properties, which provided good accuracy with reduced computing time. It was assumed that the order of convergence value, p (see Equation 2-1) is fully independent with each experimental test case because fluid properties have a very small range of variance. In addition, an INL isothermal test is being conducted with a very small density-different case calculated as $\gamma \sim 1, \gamma = \ density\ ratio\ of\ the\ low\ density\ to\ the\ heavy\ density$, which induces relatively slow stratified flow current in the channel.

Figure 2-8 compares front-head speed prediction by CFD calculation with the asymptotic approach and experiment measurement in which the CFD prediction indicates good agreement with experiment data qualitatively. In order to perform validation procedure between code prediction and experiment data, however, it is necessary to take an uncertainty concept into consideration for both the CFD code and experiment.

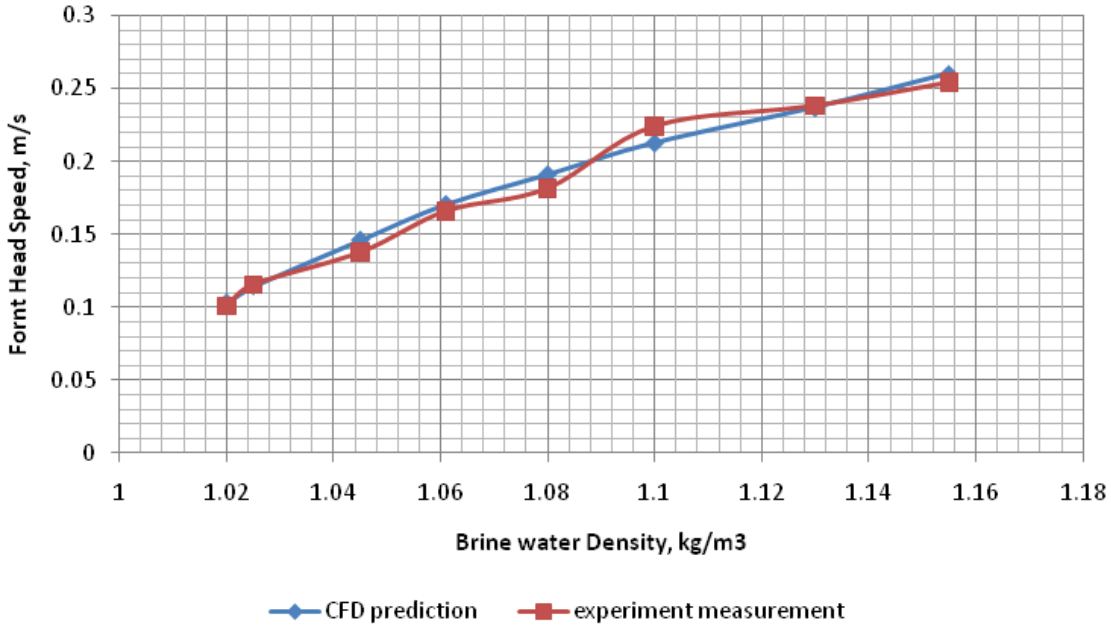

Figure 2-8. Comparison of CFD result and experiment measurement of front head speed

The linearized approximation uncertainty method (Kline and McClintonck, 1953) was used to evaluate the uncertainty of front head velocity with two measured quantities (x, t) as shown in the following mathematical procedure:

$$V = \frac{x}{t} \tag{2-11}$$

$$(dV)^2 \approx \left[\frac{\partial}{\partial x}\left(\frac{x}{t}\right)\right]^2 (dx)^2 + \left[\frac{\partial}{\partial t}\left(\frac{x}{t}\right)\right]^2 (dt)^2 \tag{2-12}$$

$$dV = \sqrt{\left[\frac{\partial}{\partial x}\left(\frac{x}{t}\right)\right]^2 (dx)^2 + \left[\frac{\partial}{\partial t}\left(\frac{x}{t}\right)\right]^2 (dt)^2} = \sqrt{\left[\left(\frac{1}{t}\right)\right]^2 (dx)^2 + \left[\left(\frac{-x}{t}\right)\right]^2 (dt)^2} \tag{2-13}$$

This method allows for calculating the uncertainty of measured front-head speed from both local and global points of view. Usually, local uncertainty from two local data points is relatively smaller than global uncertainty (with starting-point data and ending-point data). In this case, uncertainty in the distance between the start and end region is larger than that of the local region. Both cases of uncertainty were therefore calculated to obtain the mean value of experiment uncertainty for the front head speed. The uncertainties of front-head speed were also predicted for the CFD code using the asymptotic approach of the Richardson extrapolation method and GCI uncertainty error band. The uncertainties of front-head speed in the experiment and CFD code are tabulated in Table 1-4.

Table 1-4. Uncertainty of front-head speeds from experiments and CFD code calculations.

	Case 1	**Case 2**	**Case 3**	**Case 4**	**Case 5**	**Case 6**	**Case 7**	**Case 8**
Uncertainty of Experiment (%)	10.47	10.69	10.95	9.02	10.77	10.91	10.52	13.51
Uncertainty of CFD	11.08	7.34	5.42	5.07	4.10	4.03	3.44	4.45

results (%)								

4. Conclusions

Several important issues associated with the VHTR air-ingress accident were investigated and described in this paper. The isothermal experiments were twofold: (1) to understand stratified flow phenomena in the VHTR and (2) provide experimental data for validating computer codes. The isothermal experiment is focused on the three flow characteristics unique in the VHTR air-ingress accident: (1) stratified flow in the horizontal pipe, (2) stratified flow expansion at the pipe and vessel junction, and (3) stratified flow around supporting structures.

Brine and sucrose were used as heavy fluids and water was used as the light fluid. The density ratios were changed between 0.99 and 0.7. The experiment shows clear stratified flow between heavy and light fluids, even for the low-density differences.

CFD calculations were carried out for comparisons with the experimental data. As a result, the simulation result shows good agreement with the experimental data as the mesh size decreases, indicating that the current CFD code and physical models are appropriate for predicting stratified flow phenomena.

ACKNOWLEDGMENTS

This work was supported through the Department of Energy's Nuclear Hydrogen Initiative and Power Conversion Program under DOE Idaho Operations Office Contract DE-AC07-051D14517.

5. References

1. ANSYS, 2008, ICEM CFD-11.0, Manual.

2. Benjamin, T. B., 1968, "Gravity currents and related phenomena," *J. Fluid Mechanics*, Vol. 31,
pp. 209–248.

3. Bruauser, S., P. H. Emmett, and T. Teller, 1938, "Adsorption of gases in multimolecular layers," *J. Amer. Chem. Soc.*,Vol. 60, pp. 309–391.

4. Contescu, C., 2008 "Current R&D Activities on Graphite Oxidation at ORNL," Personal Communication, NGNP R&D Technical Review Meeting, Idaho National Laboratory, May 5–8, 2008.

5. Engle, G. B., 1977, *General Atomics Co. Report*, GA-A14690.

6. Eto, M. and F. B. Growcock, 1983, "Effect of oxidizing environment on the strength of H451, PGX and IG 11 graphites," *Carbon*, Vol. 21, No. 1, pp. 135–147.

7. Fagerlund, G., 1973, "Determination of specific surface by BET method," *Materjaux et Constructions*, Vol. 6, pp. 239–245.

8. Fuller, E. L., and J. M. Okoh, "Kinetics and mechanisms of the reaction of air with nuclear grade graphites: IG-110," *J. Nuclear Materials*, Vol. 240, pp. 241–250.

9. Hinsen, H. K., K. Kuhn, R. Moorman, B. Schlogl, M. Fechter, and M. Mitchel, 2008, "Oxidation experiments and theoretical examinations on graphite materials relevant for the PBMR," *Nuclear Engineering and Design*, Vol. 238, Issue 11, pp. 3018–3025.

10. Ishihara, M., T. Iyoku, T. Oku, T. Shibata, J. Sumita, 2004, "Principle Design and Data of Graphite Components," *Nuclear Engineering and Design*, Vol. 233, pp. 251–260.

11. Johnson, R. W., 2008, "Modeling strategies for unsteady turbulent flows in the lower plenum of the VHTR," *Nuclear Engineering and Design*, Vol. 238, pp. 482–491.

12. Kim, E. S., and H. C. NO, 2006, "Experimental study on the oxidation of nuclear graphite and development of an oxidation model," *Journal of Nuclear Materials*, Vol. 349, pp. 182–194.

13. Kim, E. S., H. C. NO, B. Kim, and C. H. Oh, 2007, "Estimation of Graphite and Mechanical Strength Variation of VHTR during Air-ingress Accident," *Nuclear Engineering and Design*, Vol. 238, Issue 4, pp. 837–847.

14. Kline, S. J., and F. A. McClintock, 1953, "Describing Uncertainties in Single-Sample Experiments," *Mech. Eng.*, January 1953, p. 3.

15. Liou, C. P., D. L. Parks, R. R. Schultz, and B. G. Williams, 2005, "Stratified Flows in Horizontal Piping of Passive Emergency Core Cooling Systems," *13th International Conference on Nuclear Engineering, ICONE 13-50450, Beijing, China, May 16–20, 2005*.

16. Liou, C. P., R. R. Schultz, and Y. Kukita, 1997, "Stably Stratified Flow in Closed Conduits," *Proceedings of the 5th International Conference on Nuclear Engineering, ICONE5-2024, Nice, France, May 25–29, 1997*.

17. Moorman, R., S. Alberici, H. K. Hinssen, A. K. Krussenberg, and C. H. Wu, 1999, "Oxidation behavior of carbon-based materials used for HTGRs and fusion reactors," *Adv. Sci. Technol.*, Vol. 24, pp. 331–339.

18. No, H.C., H. S. Lim, J. Kim, C. H. Oh, L. Siefken, and C. Davis, 2007, "Multi-component diffusion analysis and assessment of GAMMA code and improved RELAP 5 code," *Nuclear Engineering and Design*, Vol. 237, pp. 997–1008.

19. Ogawa, M, 1993, "Mass Transfer with Graphite Oxidation in Gas Mixture Laminar Flow through Circular Tube," *J. At. Energy Soc. Jpn.*, Vol. 35, Issue 3, p. 245.x

20. Oh, Chang H. and Eung Kim, "Air Ingress Analysis: Part 1 – Theoretical Models," *Nuclear Engineering and* Design, *Volume 241, Issue 1, January 2011, Pages 203-212*.

21. Oh, Chang H., Eung Kim, and Hyung Kang "Air Ingress Analysis: Part 2 – Computational Fluid Dynamic Models," *Volume 241, Issue 1, January 2011, Pages 213-225*.

22. Oh, C. H., C. Davis, L. Siefken, R. Moore, H. C. NO, J. Kim, G. C. Park, J. C. Lee, and W. R. Martin, 2006, *Development of Safety Analysis Codes and Experimental Validation for a Very High Temperature Gas-Cooled Reactor, Final Report*, INL/EXT-06-01362, Idaho National Laboratory, March 2006.

23. Oh, C. H., E. S. Kim, H. C. NO, and N. Z. Cho, 2008, *Experimental Validation of Stratified Flow Phenomena, Graphite Oxidation, and Mitigation Strategies of Air Ingress Accident, FY 2008 Report,* INL/EXT-08-14840, Idaho National Laboratory, December 2008.

24. Oh, C. H., E. S. Kim, S. Kang Hyung, H. C. NO, and N. Z. Cho, 2009, *Experimental Validation of Stratified Flow Phenomena, Graphite Oxidation, and Mitigation Strategies of Air Ingress Accident, FY 2008 Report*, INL/EXT-09-16465, Idaho National Laboratory, December 2009.

25. Roache, P. J., 1998, *Verification and Validation in Computational Science and Engineering*, Hermosa Publishers, Albuquerque, New Mexico, 1998.

26. Schultz, R. R., *et al.*, 2006, *Next Generation Nuclear Plant Methods Technical Program Plan*, INL/EXT-06-11804, September 2006.

27. Simpson, J. E., and R. E. Britter, 1979, "The dynamics of the head of a gravity current advancing over a horizontal surface," *J. Fluid Mech.*, Vol. 94, Part 3, pp. 477–495, 1979.

28. Takeda T., 1997, *Air Ingress Behavior during a Primary-pipe Rupture Accident of HTGR*, JAERI-1338, Japan Atomic Energy Research Institute, 1997.

29. Takeda, T. and M. Hishida, 1996, "Studies on Molecular Diffusion and Natural Convection in a Multicomponent Gas System," *International Journal of Heat and Mass Transfer*, Vol. 39, No. 3, pp. 527–536, 1996.

30. Wichner, R. P., 1976, *Oak Ridge National Laboratory Report*, ORNL/TM-5534.

31. Yan, *et al.*, 2008, "A Study of Air Ingress and its Prevention in HTGR," *Nuclear Technology*, Vol. 163, September 2008.

32. Yih, C. S., 1980, *Dynamics of Nonhomogeneous Fluids*, Macmillan.